TU Delft

Delft University of Technology

A comparison of steam reforming concepts in solid oxide fuel cell systems

van Biert, L.; Visser, K.; Aravind, P. V.

DOI
10.1016/j.apenergy.2020.114748

Publication date
2020

Document Version
Final published version

Published in
Applied Energy

Citation (APA)
van Biert, L., Visser, K., & Aravind, P. V. (2020). A comparison of steam reforming concepts in solid oxide fuel cell systems. *Applied Energy*, *264*, Article 114748. https://doi.org/10.1016/j.apenergy.2020.114748

Important note
To cite this publication, please use the final published version (if applicable).
Please check the document version above.

Copyright
Other than for strictly personal use, it is not permitted to download, forward or distribute the text or part of it, without the consent of the author(s) and/or copyright holder(s), unless the work is under an open content license such as Creative Commons.

Takedown policy
Please contact us and provide details if you believe this document breaches copyrights.
We will remove access to the work immediately and investigate your claim.

This work is downloaded from Delft University of Technology.
For technical reasons the number of authors shown on this cover page is limited to a maximum of 10.

Applied Energy 264 (2020) 114748

Contents lists available at ScienceDirect

Applied Energy

journal homepage: www.elsevier.com/locate/apenergy

A comparison of steam reforming concepts in solid oxide fuel cell systems

L. van Biert[a,b,*], K. Visser[a], P.V. Aravind[b]

[a] Department of Maritime & Transport Technology, Delft University of Technology, Mekelweg 2, 2628 CD Delft, the Netherlands
[b] Department of Process & Energy, Delft University of Technology, Leeghwaterstraat 39, 2628 CB Delft, the Netherlands

HIGHLIGHTS

- Different steam reforming concepts are analysed at both stack and system level.
- System configurations with allothermal and adiabatic pre-reforming are compared.
- Steam supply through water and anode off-gas recirculation are compared.
- Allothermal pre-reforming and water recirculation yield the highest efficiency.
- High stack efficiencies do not necessary result in high system efficiencies.

ARTICLE INFO

Keywords:
Solid oxide fuel cell
Allothermal reforming
Adiabatic reforming
Water recirculation
Anode off-gas recirculation
Thermal stress

ABSTRACT

Various concepts have been proposed to use hydrocarbon fuels in solid oxide fuel cell (SOFC) systems. A combination of either allothermal or adiabatic pre-reforming and water recirculation (WR) or anode off-gas recirculation (AOGR) is commonly used to convert the fuel into a hydrogen rich mixture before it is electrochemically oxidised in the SOFC. However, it is unclear how these reforming concepts affect the electrochemistry and temperature gradients in the SOFC stack. In this study, four reforming concepts based on either allothermal or adiabatic pre-reforming and either WR or AOGR are modelled on both stack and system level. The electrochemistry and temperature gradients in the stack are simulated with a one-dimensional SOFC model, and the results are used to calculate the corresponding system efficiencies. The highest system efficiencies are obtained with allothermal pre-reforming and WR. Adiabatic pre-reforming and AOGR result in a higher degree of internal reforming, which reduces the cell voltage compared to allothermal pre-reforming and WR. Although this lowers the stack efficiency, higher degrees of internal reforming reduce the power consumption by the cathode air blower as well, leading to higher system efficiencies in some cases. This illustrates that both stack and system operation need to be considered to design an efficient SOFC system and predict potentially deteriorating temperature gradients in the stack.

1. Introduction

Global efforts to reduce the emissions of greenhouse gases and hazardous air pollutants call for the development of clean and efficient energy conversion technologies [1,2]. Electrochemical conversion of electricity into hydrogen trough electrolysis and to electricity with fuel cells enables clean and efficient transport, storage and use of renewable energy [3,4]. However, the low volumetric energy density of current hydrogen storage technologies may result in unpractically large fuel tanks in applications with long independent mission requirements, for example intercontinental air traffic and shipping [5]. Synthetic fuels with a higher volumetric energy density, such as alkanes, alcohols or ethers may offer a better alternative for those applications [6].

Hydrocarbon fuels are usually converted into a hydrogen rich mixture before they can be electrochemically oxidised in a fuel cell [7]. Steam reforming, an endothermic reaction which requires heat and steam, is often used because it yields most hydrogen [8]. High temperature solid oxide fuel cells (SOFCs) produce high temperature heat and steam in the electrochemical oxidation reaction that can be used for this purpose, enhancing heat integration and the overall system efficiency. Therefore, SOFC systems fuelled with natural gas or biogas can achieve electrical efficiencies of 65% based on the lower heating value (LHV) in stand-alone operation and even in excess of 70% when combined with gas turbines, steam turbines or reciprocating engines [9,10].

The reforming reaction may proceed directly on the SOFC anode [11]. Direct internal reforming (DIR) further improves heat integration

* Corresponding author at: Department of Maritime & Transport Technology, Delft University of Technology, Mekelweg 2, 2628 CD Delft, the Netherlands.
E-mail address: l.vanbiert@tudelft.nl (L. van Biert).

https://doi.org/10.1016/j.apenergy.2020.114748
Received 19 November 2019; Received in revised form 1 February 2020; Accepted 26 February 2020
Available online 09 March 2020
0306-2619/ © 2020 The Author(s). Published by Elsevier Ltd. This is an open access article under the CC BY license (http://creativecommons.org/licenses/BY/4.0/).

Nomenclature

Acronyms

AC	alternating current
AOGR	anode off-gas recirculation
DC	direct current
DIR	direct internal reforming
ESC	electrolyte supported cell
GDC	gadolinium doped cerium oxide
IC	interconnect
ISM	integrated stack module
LHV	lower heating value
LSM	lanthanum strontium manganite
MSR	methane steam reforming
OC	oxygen-to-carbon
PEN	positive electrode-electrolyte-negative electrode assembly
PI	proportional and integral gain
SOFC	solid oxide fuel cell
WR	water recirculation
YSZ	yttrium stabilised zirconium oxide

Greek symbols

α	global electrochemical reaction order [–]
η	efficiency [–]
$\hat{\eta}$	electrochemical overpotential [V]
ι	tortuosity factor [–]
λ	thermal conductivity [$\mathrm{W\,m^{-1}\,K^{-1}}$]
ρ	density [$\mathrm{kg\,m^{-3}}$]
σ	electrical conductivity [$\mathrm{S\,m^{-1}}$]
τ	thickness [m]
ε	porosity [$\mathrm{m^3\ m^{-3}}$]

Roman symbols

$\bar{A}$	pre-exponential adsorption factor [$\mathrm{bar^{-x}}$]
c_p	heat capacity [$\mathrm{J\,mol^{-1}\,K^{-1}}$]
E_a	activation energy [$\mathrm{J\,mol^{-1}}$]
$\Delta\bar{H}$	enthalpy change of adsorption [$\mathrm{J\,mol^{-1}}$]
I	current [A]
j	current density [$\mathrm{A\,m^{-2}}$]
$\bar{K}$	adsorption constant [$\mathrm{bar^{-x}}$]
$\hat{k}_0$	pre-exponential factor exchange current density [$\mathrm{A\,m^{-2}}$]
k	reaction rate constant [$\mathrm{mol\,Pa^x\,s^{-1}\,m^{-2}}$]
k_0	pre-exponential factor reaction constant [$\mathrm{mol\,Pa^x\,s^{-1}\,m^{-2}}$]
l	longitudinal coordinate [m]
N	number [–]
p	pressure [bar]
$\dot{Q}$	heat flux [W]
$\dot{q}$	relative heat loss [–]
Q	reaction quotient [–]
$\bar{R}$	universal gas constant [$\mathrm{J\,mol^{-1}\,K^{-1}}$]
$\bar{r}$	mean pore radius [m]
RR	recirculation ratio [–]
T	temperature [°C]
U	voltage [V]
$\dot{V}$	volumetric flow [$\mathrm{Nl\,min^{-1}}$]
w	width [m]

Superscripts

in	inlet
out	outlet

Subcripts

0	reference
aa	active area
act	activation
an	anode
aux	auxiliary
ca	cathode
ch	channel
conc	concentration
cv	control volume
el	electrolyte
eva	evaporator
f	fuel
gl	global
hex	heat exchanger
i	species *i*
ins	insulation
is	isentropic
m	mechanical
ms	moisture separator
ohm	ohmic
pr	pre-reformer
ref	reformer
sp	single pass

in the system, since the heat and steam produced in the hydrogen oxidation reaction are directly used to reform the fuel. In addition, the endothermic reforming reaction reduces the cathode air flow required to cool the SOFCs, which limits the parasitic power consumption from the air blower [12]. Internal reforming of natural gas is most common in SOFC systems today, but other fuels can be converted internally as well. This includes, for example, internal reforming of methanol [13], ethanol [11], dimethyl ether [14] and other hydrocarbons [15], but also cracking of ammonia [16].

Although DIR seems beneficial from a system integration perspective, it may compromise the electrochemical reactions and increase thermal stresses in the SOFC stack [17]. The endothermic steam reforming reaction typically occurs primarily at the entrance of the stack, where the methane partial pressure is high, while the exothermic hydrogen oxidation reaction will be most prominent at the hot outlet part of the stack. This reduces the temperature at the inlet of the stack, which in turn increases the temperature gradient and electrochemical losses [18].

The challenges introduced by DIR can be mitigated by partially pre-reforming the fuel. To drive the reforming reaction, heat and steam have to be supplied to an external pre-reformer. Rather than producing them externally, both heat and steam can be obtained from the exhaust gases of the SOFC to enhance the overall system efficiency. Two types of pre-reforming are commonly employed in SOFC systems:

- Adiabatic reforming, for which only the heat available in the reactive flow is used and the temperature reduces due to the endothermic reforming reaction;
- Allothermal reforming, in which a constant reformer temperature is maintained with heat supplied from an external source, for example from hot exhaust gases.

Similarly, steam is often supplied by either of the following two methods:

- Water recirculation (WR), where water is condensed from exhaust

gas, evaporated and mixed with the fresh fuel;
- Anode off-gas recirculation (AOGR), where a part of the anode outlet gas is recirculated and mixed with the fresh fuel.

Combining these options yields four different pre-reforming concepts in SOFC systems, shown in Table 1.

The anode and cathode outlet gases of the SOFC are usually mixed and passed through a catalytic burner, which generates steam and increases the temperature of the outlet gases further. The hot flue gas can be used to supply heat to both an allothermal pre-reformer and evaporator. Water can be subsequently condensed from the cooled exhaust gases, evaporated and mixed with the fresh fuel for WR [19,20].

Although allothermal pre-reforming and WR offer a simple method to utilise hydrocarbon fuels in SOFC systems, a substantial amount of useful heat may be destroyed in the evaporator, pre-reformer and preheaters, which compromises heat available for consumers or thermal bottoming cycles [10]. Alternatively, the heated allothermal pre-reformer may be replaced by an adiabatic reformer, which reduces fuel conversion and heat demand. WR can be avoided by recirculating a part of the steam-containing anode outlet gas [19].

AOGR omits the need for a condenser and evaporator and may result in more homogenous conditions in the stack. Anode off-gas can be recirculated with blowers, but there are few products readily available which can withstand the high gas temperatures and achieve an acceptable lifetime [21]. In addition, the amount of recirculated anode off-gas determines the oxygen-to-carbon ratio gas entering the pre-reformer, which should be sufficiently high to avoid carbon formation [22]. The amount of anode off-gas that needs to be recirculated to suppress carbon formation depends on the temperature and fuel gas composition, which is in turn affected by the overall fuel utilisation [23]. Chen et al. [24] show how anode and cathode off-gas recirculation can be used to control the stack inlet temperatures in an SOFC-GT combined cycle system.

Ejectors offer an alternative for high temperature AOGR in SOFCs without moving parts, but are more difficult to control [25,26]. Genc et al. [27] study the optimal ejector operating pressure for an SOFC system with AOGR. The geometry of the ejector is subsequently optimised in a follow-up study [28]. Polverino et al. [29] demonstrate the application of a model-based diagnostic technique to isolate faults in a SOFC system with AOGR.

Another option is low temperature AOGR, in which the hot effluents from the anode exhaust are cooled down, recirculated at low temperature, and heated up again [17,19,25]. Net electrical efficiencies in 60% LHV are projected for such a system developed by Powell et al. [17]. Moreover, the authors argue that the combination of adiabatic pre-reforming and low temperature AOGR used in their system reduces thermal quenching in the stack.

DIR in SOFC stacks has been modelled in several studies. Kupecki et al. [30–32] simulate DIR with a quasi-1D model and validate the current-voltage characteristics for two reformate compositions. Greco et al. [33] and Sorce et al. [34] perform studies on a similar stack to simulate faulty operating states. However, the kinetics of the DIR reaction as well as the influence of heat transfer effects in the inactive area of the stack appear to be not considered in these studies.

Peters et al. [19] evaluated the potential combined heat and power efficiency of several system layouts with AOGR thermodynamically. However, the reforming and electrochemical reactions in the SOFC are not modelled in detail, while different reforming concepts may be expected to affect the stack performance as well. Therefore, the implications of different reforming concepts on the efficiency, power density and thermal stresses of the stack are not considered.

In this study, the effect of different reforming concepts in SOFC systems on both stack and the system is analysed. Methane is used as a model fuel, but the results are relevant for other organic compounds as well, since methane is commonly present in the reformates of those fuels [35,36]. Stack operation is simulated with a 1D DIR SOFC model and methane steam reforming (MSR) kinetics developed in previous work [18,37]. System models are developed in analogy to previous work [10]. The models are developed in the in-house developed flow sheet program Cycle-Tempo, which incorporates a library of built-in thermodynamic component models. The program can be used to calculate mass, energy and exergy balances in thermodynamic cycles [38,39].

The stack simulations are used to obtain the electrochemical characteristics of the SOFC for different system configurations and operating conditions, such as temperatures, fuel compositions and fuel utilisations. In addition, the temperature gradients are reported as they are an indicator for the thermal stresses in the stack, which affect the lifetime of the SOFC. The current-voltage characteristics are then used in system models to calculate the efficiency of the investigated system concepts for various fuel utilisations, nominal operating conditions and either a constant stack power or maximum stack efficiency.

2. Reforming concepts

The reforming concepts shown in Table 1 are studied in detail through stack and system simulations. Exemplary system layouts are defined for all four options to analyse and compare the investigated concepts.

2.1. Allothermal pre-reforming and water recirculation

The first reforming concept, shown in Fig. 1a, is a conventional option based on allothermal reforming and WR. The fresh fuel is mixed with steam and partially reformed in an allothermal pre-reformer, heated with hot flue gas from the off-gas burner. In addition, the flue gas is used to pre-heat the cathode air and evaporate water, condensed from the cooled exhaust gases.

2.2. Allothermal pre-reforming and anode off-gas recirculation

The second concept, shown in Fig. 1b, combines allothermal pre-reforming with AOGR. Similar to the previous configuration, the hot off-gas burner exhaust gas is used to heat the allothermal pre-reformer. However, a part of the anode off-gas is recirculated to provide steam for reforming. In addition, the gases are cooled down to a temperature of 120 °C to avoid high temperature AOGR. The layout is based on a low temperature AOGR configuration proposed by Engelbracht et al. [25].

Table 1
Overview of different reforming strategies, with heat and steam either provided directly by the electrochemical reaction (AOGR and adiabatic reforming) or indirectly from the exhaust gases (WR and allothermal reforming).

		Steam		
		exhaust	anode	notes
Heat	exhaust	WR and allothermal reforming	AOGR and allothermal reforming	low u_{ox} complete combustion
	anode	WR and adiabatic reforming	AOGR and adiabatic reforming	high u_{ox} uncombusted effluents
	notes	$u_{f,sp} = u_{f,gl}$ water trap, pump and evaporator	$u_{f,sp} < u_{f,gl}$ recirculation blower or ejector	

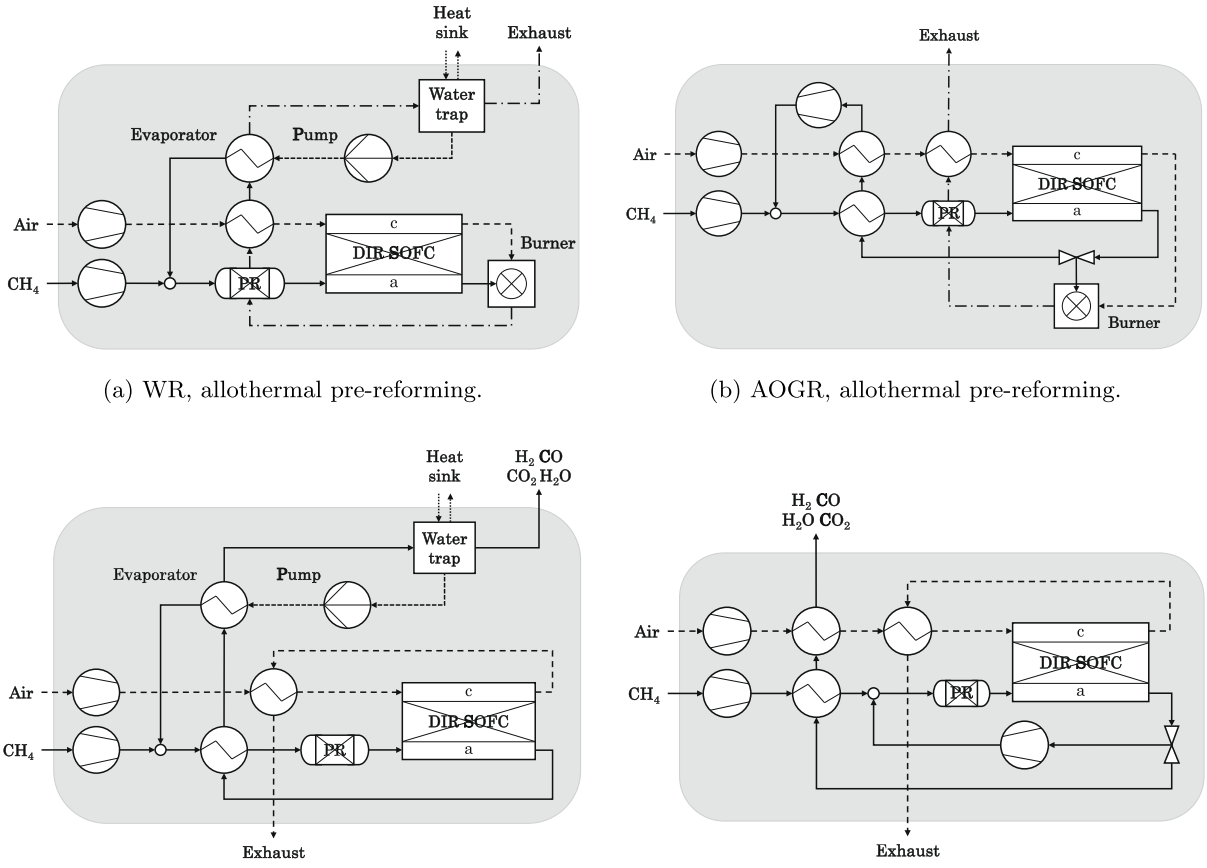

(a) WR, allothermal pre-reforming.

(b) AOGR, allothermal pre-reforming.

(c) WR, adiabatic pre-reforming.

(d) AOGR, adiabatic pre-reforming.

Fig. 1. Flow sheets of the investigated reforming configurations.

2.3. Adiabatic pre-reforming and water recirculation

The third reforming concept omits the use of an off-gas burner entirely. Instead, the mixture of fuel and steam is only pre-heated and passed through an adiabatic pre-reformer. Similar to the first configuration, steam is condensed from the anode-off gas, evaporated and mixed with the fuel. However, steam can be condensed more easily in this configuration, since the anode off-gas is not mixed with cathode air and has a steam concentration. Moreover, the un-burned fuel, consisting of hydrogen and carbon monoxide may be further utilised in other utilities, for example in combined heat, hydrogen and power production, low temperature fuel cells or thermal bottoming cycles [10].

2.4. Adiabatic pre-reforming and anode off-gas recirculation

The last reforming concept uses the heat and steam produced by the electrochemical reaction only, combining high temperature AOGR and adiabatic pre-reforming. A part of the anode off-gas is recycled, while the remaining part is used to pre-heat both fuel and air. Heat from the cathode air is recuperated as well, but the remaining energy in the exhaust gases can be used in other applications. Similar configurations have been proposed in several studies, although some use ejectors instead of high temperature recirculation blowers [26].

3. Modelling and simulation

Both stack and system models are used to investigate the implications of different reforming concepts on SOFC systems. Section 3.1 discusses the calculation of anode inlet compositions and temperatures for different system configurations and operating conditions. The calculated anode inlet conditions are then used to simulate the corresponding current-voltage characteristics of and temperature gradients in the SOFC stack with a dynamic model, described in Section 3.2. The cell voltages calculated with the stack model are then implemented in corresponding system models discussed in Section 3.4. Section 3.3 summarises the overall simulation procedure and simulated conditions.

3.1. Anode inlet composition and temperature

The composition and temperature of the fuel flow entering the anode compartment of the SOFC vary for different system configurations and operating conditions. For example, the composition depends on the ratio of steam or recirculated anode flow to the fresh fuel flow for the WR and AOGR concepts respectively. Similarly, the anode inlet temperature is equal to the reformer temperature for allothermal pre-reforming, but follows from thermodynamic equilibrium calculation in case of adiabatic pre-reforming.

The anode inlet compositions and temperatures are calculated assuming that the flow is in chemical equilibrium at the anode inlet. The chemical equilibrium composition is calculated through Gibbs free energy minimisation. This is solved iteratively for adiabatic reforming, since the equilibrium composition is a function of the outlet temperature, while the outlet temperature in turn follows from an energy balance resulting from the equilibrium composition.

For the AOGR cases, an appropriate amount of recirculation has to be selected. The reforming ratio is adjusted for different global fuel utilisations ($u_{f,gl}$) in this study, to maintain a constant oxygen-to-carbon (OC) ratio. The amount of recirculation required can be shown to follow from

$$RR = \frac{\dot{n}_{recycle}}{\dot{n}_{an}^{out}} = \frac{\text{OC ratio}}{(2C + H/2 - O)u_{f,gl}}, \quad (1)$$

where C, H and O are the number of carbon, hydrogen and oxygen atoms in an average fresh fuel molecule respectively. The effective fuel utilisation in the stack decreases for higher recirculation ratios, and the fuel utilisation for a single pass follows from from:

$$u_{f,sp} = \frac{u_{f,gl}(1 - RR)}{1 - RR\,u_{f,gl}} \quad (2)$$

Whether carbon formation is thermodynamically favourable depends on the temperature, pressure and fractions of carbon, hydrogen and oxygen in the fuel. This can be visualised in a CHO ternary phase diagram, shown in Fig. 2. The black lines indicate the region where solid carbon formation is thermodynamically expected (C(s) + gas) for 500, 600 and 700 °C, while the grey lines represent constant OC ratios in the fuel mixture of 1.5, 2 and 2.5. The dash-dotted lines show how the carbon, hydrogen and oxygen fraction of methane are changing when diluted with either WR or AOGR.

Fig. 2 shows that carbon formation is thermodynamically not favourable when WR is used and the OC ratio is above 1.5. For AOGR, however, OC ratios in excess of 2.5 are required to ensure that carbon deposition is thermodynamically not expected at a temperature of 500 °C. Whether carbon depositing will indeed occur depends on the type of carbon formed and the individual reaction kinetics of carbon depositing and removal reactions [40]. For example, Halinen et al. [23] observed no carbon depositing 600 °C for conditions where it was thermodynamically expected.

3.2. Stack modelling

The stack is simulated with a 1D dynamic model developed in previous work [18]. The stack model represents the Staxera/Sunfire ISM V3.3, equipped with two Mk200 stacks placed on top of each other, making a total of 60 cells [41,42]. Fuel and air manifolding are integrated in the stack and ISM respectively. The Mk200 stacks are equipped with ESC2 cells from Kerafol/H.C. Starck with a nickel-gadolinium doped cerium oxide (Ni-GDC) anode, yttrium stabilised zirconia (3YSZ) electrolyte and 8YSZ/lanthanum strontium manganese (LSM)-LSM double layer cathode. A schematic overview of the ISM is shown in Fig. 3a.

The stack is modelled as a 1D plug flow reactor with individual temperature layers for air, fuel, positive electrode-electrolyte-negative electrode (PEN) assembly and the interconnect, all discretised in the flow direction. A schematic overview of the modelling approach is shown in Fig. 3b. The main dimensions, properties and operating conditions of the ISM are obtained in previous work and are summarised in Table 2 [18].

Periodic boundary conditions are imposed on the interconnect, effectively assuming an infinitely repeated stack assembly. A Newton boundary condition is applied to the interconnects to account for convective heat transfer to the environment, similar to Greco et al. [33]. In contrast to models used in other studies, the model in this study accounts for heat transfer between the anode and cathode compartments in the inactive in- and outflow sections of the stack as well.

The electrochemical model was validated with power curves reported by the manufacturer in previous work [18]. The current voltage characteristics are calculated with the equipotential assumption

$$U_{cell} = U_{Nernst} - \hat{\eta}_{ohm} - \hat{\eta}_{conc} - \hat{\eta}_{act}, \quad (3)$$

where the equilibrium potential U_{Nernst} for hydrogen is used, assuming that hydrogen oxidation is the dominating electrochemical reaction. The ohmic and concentration overpotential losses are calculated based on a method described by Aguiar et al. [43]. The activation overpotentials are calculated form a modified version of the power law proposed by Costamagna et al. [44]:

$$\hat{\eta}_{act} = \frac{\bar{R}T}{F} sinh^{-1}\left(\frac{j}{2j_0}\right) \quad (4)$$

$$j_{0,ca} = \hat{k}_{0,ca}\,\alpha_{O_2}^{1/4}\,exp\left(-\frac{E_{a,ca}}{\bar{R}T}\right) \quad (5)$$

$$j_{0,an} = \hat{k}_{0,an}\,\alpha_{H_2}^{1/2}\,exp\left(-\frac{E_{a,an}}{\bar{R}T}\right), \quad (6)$$

where α_i is the activity of species i. The reaction orders in Eqs. (5) and (6) and the corresponding electrochemical parameters, given in Table 3, were shown to result in accurate predictions ($R^2 = 0.99$) of the

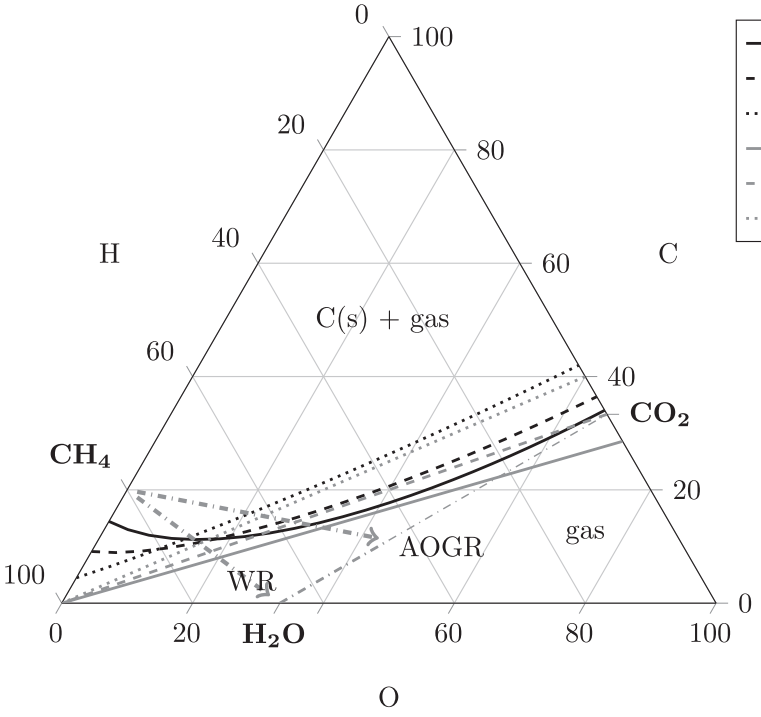

Fig. 2. Ternary phase diagram for carbon, hydrogen and oxygen, with the region. The grey lines indicate constant OC ratios in the fuel mixture, for which carbon formation is thermodynamically expected when the composition is below the black lines for different temperatures. The composition of different reformates can be identified by following the arrows from pure methane (CH_4) to steam (H_2O) for WR and oxygen for AOGR.

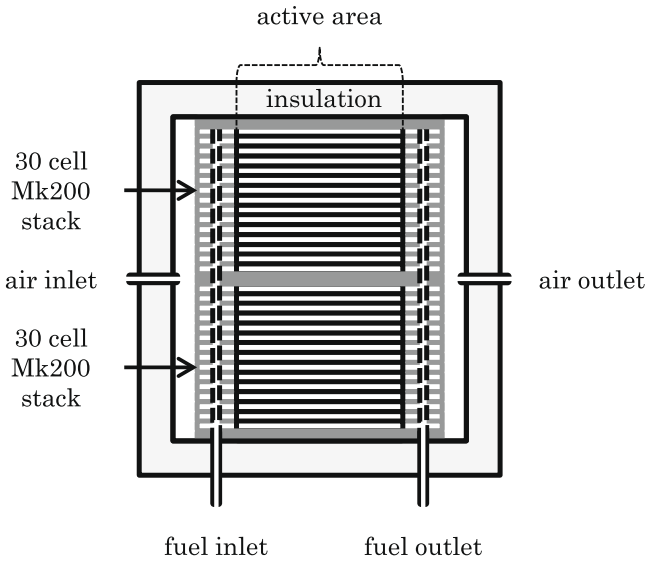

(a) Sunfire/Staxera ISM V3.3.

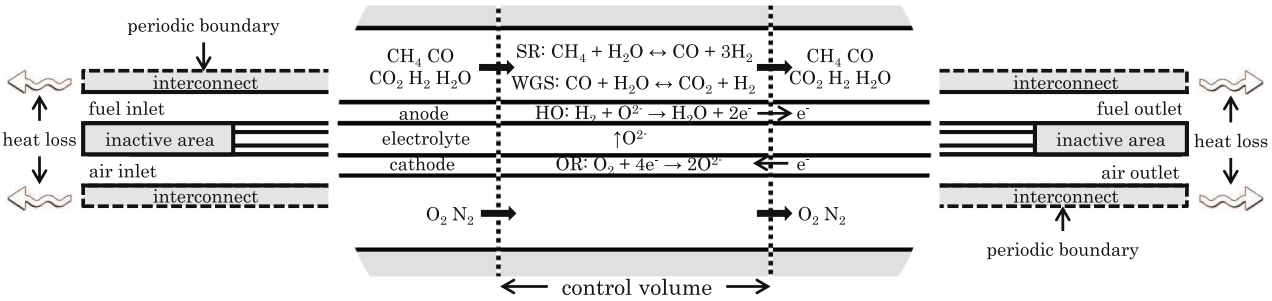

(b) 1D stack model overview.

Fig. 3. Schematic representation of the Sunfire/Staxera ISM V3.3 and overview of the 1D stack model.

current-voltage characteristics of the stack for three different fuel compositions: hydrogen-nitrogen, catalytic partial oxidation and steam reformate [18].

It was shown in previous work that an appropriate description of the internal MSR kinetics yields a more realistic prediction of the spatial variation in the DIR rate from inlet to outlet [18]. Therefore, MSR kinetics were derived on the same type of ESC2 cells with Ni-GDC anodes in single cell experiments carried out in a follow-up study [37]. These are of the classical Langmuir-Hinshelwood type, assuming accusative adsorption of methane and dissociative adsorption of steam respectively:

$$r_{MSR} = \frac{k\,K_{CH_4}\,K_{H_2O}\,p_{CH_4}\sqrt{p_{H_2O}}}{(1 + K_{CH_4}p_{CH_4} + K_{H_2O}\sqrt{p_{H_2O}})^2}\left(1 - \frac{Q}{K_{MSR}}\right), \tag{7}$$

where p_i is the partial pressure of species i, Q is the reaction quotient and K_{MSR} the MSR equilibrium constant. The reaction and adsorption constants are calculated from the Arrhenius and van 't Hoff relation respectively:

$$k = k_0\,exp\left(-\frac{E_a}{\bar{R}T}\right) \tag{8}$$

$$\bar{K}_i = \bar{A}_i\,exp\left(-\frac{\Delta\bar{H}_i}{\bar{R}T}\right) \tag{9}$$

The parameters for these MSR kinetics are included in Table 3.

3.3. System modelling

System models are developed in the in-house developed thermodynamic flow-sheet calculation program Cycle-Tempo for each configuration. The Cycle-Tempo package incorporates built-in thermodynamic component models of pumps, blowers, heat exchangers, evaporators, moisture separators, reformers, combustors and fuel cells [38,39]. The system of equations is subsequently solved to calculate pressures, flows and temperatures in every system node. These are then used to calculate the gross and net system efficiencies.

The SOFC is modelled as an allothermal ideal plug flow reactor in Cycle-Tempo, assuming that the reforming and water gas shift reactor are in equilibrium. However, the user can provide various SOFC parameters for off-design calculations, and this is used to implement the cell voltages calculated with the 1D dynamic stack model in the system models. However, the remaining operating conditions, such as mass flows, temperatures and pressure drop are calculated with the system models, and the heat loss from the ISM to the environment, $\dot{Q}_{loss}$, is calculated relative to the electric power produced by the stack:

$$\dot{Q}_{loss} = \dot{q}_{loss}\,P_{SOFC,DC} \tag{10}$$

Chemical equilibrium is assumed in the pre-reformer, and complete combustion in the off-gas burner. The losses in rotating equipment are calculated from their isentropic and mechanical efficiencies. The flue gas leaving the moisture separator is assumed to be saturated at 25 °C. An overview all parameters used in the system analysis is provided in Table 4.

Table 2
Parameter derived in earlier work for the ISM V3.3 from Sunfire/Staxera with ESC2 cells from Kerafol/H.C. Starck [18,41,42].

Geometric properties	Units	Value
No. of cells, N_{cells}	[–]	60
Cell length, l_{cell}	[m]	0.164
Active area length, l_{aa}	[m]	0.09
Cell width, w_{cell}	[m]	0.142
No. of channels, N_{ch}	[–]	24
Channel height, τ_{ch}	[m]	$1{\cdot}10^{-3}$
Electrolyte thickness, τ_{el}	[m]	$90{\cdot}10^{-6}$
Anode thickness, τ_{an}	[m]	$35{\cdot}10^{-6}$
Cathode thickness, τ_{ca}	[m]	$35{\cdot}10^{-6}$
Interconnect thickness, τ_{IC}	[m]	$500{\cdot}10^{-6}$
No. of control volumes, N_{cv}	[–]	$50+(2\times21)$
Thermal properties		
PEN density, ρ_{PEN}	[kg m^{-3}]	5900
PEN heat capacity, $c_{p,PEN}$	[J kg^{-1} K^{-1}]	500
PEN thermal cond., λ_{PEN}	[J m^{-1} s^{-1} K^{-1}]	2
IC density, ρ_{IC}	[kg m^{-3}]	8000
IC heat capacity, $c_{p,IC}$	[J kg^{-1} K^{-1}]	500
IC thermal cond., λ_{IC}	[J m^{-1} s^{-1} K^{-1}]	24
Ins. thermal cond., λ_{ins}	[J s^{-1} K^{-1}]	$2.91{\cdot}10^{-3}$
Electrolyte and electrode properties		
Electrolyte conductivity, σ_{el}	[Ω^{-1} m^{-1}]	$20.5{\cdot}10^{3}\ \exp(-\ 9.03{\cdot}10^{3}/T)$
Anode conductivity, σ_{an}	[Ω^{-1} m^{-1}]	$30.3{\cdot}10^{3}$
Cathode conductivity, σ_{ca}	[Ω^{-1} m^{-1}]	$12.9{\cdot}10^{3}$
Contact resistance, $R_{contact}$	[Ω m^2]	$5{\cdot}10^{-6}$
Electrode porosity, ε	[–]	0.3
Electrode tortuosity factor, ι	[–]	6
Electrode pore radius, $\bar{r}$	[m]	$5{\cdot}10^{-7}$
Operating parameters		
Max PEN temperature, T_{PEN}^{max} (achieved through cathode air flow control)	[°C]	850
Min air flow, $\dot{V}_{ca}^{min}$	[Nl min^{-1}]	40
Max stack current, I_{stack}^{max}	[A]	30
Min stack voltage, U_{stack}^{min}	[V]	36

Table 3
Overview of the parameters used in the kinetic models of the reforming and electrochemical reactions, derived in previous work [18,37].

Reforming parameters	Units	Value
MSR rate constant, $k_{0,MSR}$	[mol s^{-1} m^{-2}]	$1.467{\cdot}10^{10}$
Activation energy, E_a	[J mol^{-1}]	$207.6{\cdot}10^{3}$
CH_4 pre-exponental factor, $\bar{A}_{CH4}$	[bar^{-1}]	$4.2{\cdot}10^{-3}$
CH_4 adsorption enthalpy, $\Delta\bar{H}_{CH4}$	[J mol^{-1}]	$-\ 54.76{\cdot}10^{3}$
H_2O pre-exponental factor, $\bar{A}_{H_2O}$	[bar$^{-0.5}$]	$1.9{\cdot}10^{-3}$
H_2O adsorption enthalpy, $\Delta\bar{H}_{H_2O}$	[J mol^{-1}]	$-\ 62.17{\cdot}10^{3}$
Electrochemical parameters		
Cathode pre-exponential factor, $\hat{k}_{0,co}$	[A m^{-2}]	$7{\cdot}10^{8}$
Cathode activation energy, $E_{a,ca}$	[J mol^{-1}]	$120{\cdot}10^{3}$
Anode pre-exponential factor, $\hat{k}_{0,an}$	[A m^{-2}]	$1.81{\cdot}10^{9}$
Anode activation energy, $E_{a,an}$	[J mol^{-1}]	$120{\cdot}10^{3}$

3.4. Stack and system simulations

Two types of models are used to study the implications of different reforming concepts. Stack simulations provide detailed insight in the effect of different reforming concepts on the SOFC, and the results are used in system models to calculate the overall system efficiencies. The overall simulation procedure is as follows:

1. The anode inlet compositions and temperatures are calculated for different system configurations and operating conditions;
2. The anode inlet compositions and temperatures are used to simulate current voltage characteristics of and temperature gradient in the stack for different system configurations and operating conditions;
3. The simulated cell voltages are implemented in the system models to calculate the overall system efficiencies for nominal operating conditions, a range of global fuel utilisations and:
   (a) A constant stack power of 1 kWe, which is achieved at different voltages for the investigated reforming concepts;
   (b) The maximum cell voltage, achieved at the minimum stack current required to sustain the stack temperature for the minimum cathode air flow of 40 Nl min^{-1}.

Table 4
Overview of the parameters used in the system model, based on previous work and stack manufacturer specifications [10].

System parameter	Units	Value
Stack outlet temperature, T_{stack}^{out}	[°C]	825
Air inlet temperature, T_{air}^{in}	[°C]	725
Allothermal pre-reformer temperature, T_{ref}	[°C]	600
Adiabatic pre-reformer inlet temperature, T_{ref}^{in}	[°C]	775
Evaporator outlet temperature, T_{eva}^{out}	[°C]	120
LT-AOGR blower inlet temperature, T_{blower}^{in}	[°C]	120
Moisture separator temperature, T_{ms}^{out}	[°C]	25
Anode pressure drop, Δp_{an}	[bar]	0.03
Cathode pressure drop, Δp_{ca}	[bar]	0.05
Heat exchanger pressure drop, Δp_{hex}	[bar]	0.02
Pre-reformer pressure drop, Δp_{pr}	[bar]	0.02
Off-gas burner pressure drop, Δp_{burner}	[bar]	0.02
Relative heat loss, $\dot{q}_{loss}$	[–]	0.2
Isentropic efficiency blower, $\eta_{is,blower}$	[–]	0.7
Mechanical efficiency blower, $\eta_{m,blower}$	[–]	0.8
Isentropic efficiency pump, $\eta_{is,pump}$	[–]	0.85
Mechanical efficiency pump, $\eta_{m,pump}$	[–]	0.9
Inverter efficiency, $\eta_{inverter}$	[–]	0.95

Fig. 4 shows a schematic overview of this simulation process.

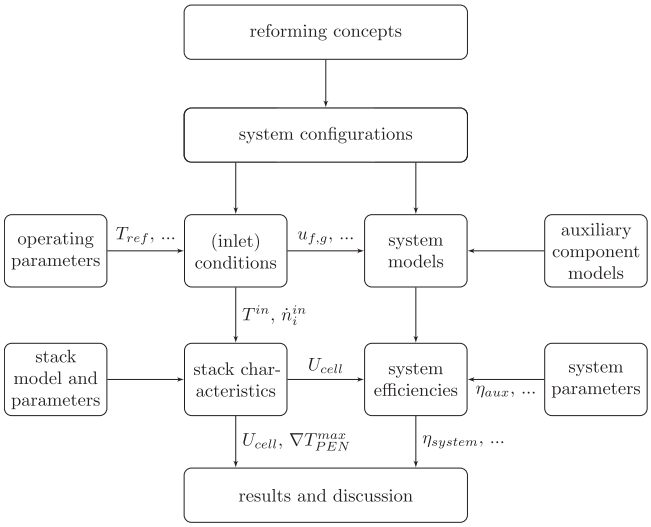

Fig. 4. Flowchart of the procedure used to simulate the investigated reforming concepts.

3.4.1. Stack simulations

The current voltage characteristics are determined by simulating stack operation for each of the investigated configuration. The stack performance is mapped by increasing the stack current from 15 to 27 A for various stack currents and global fuel utilisations. Additional off-design operating conditions are simulated by changing the OC ratio, cathode air inlet temperature and pre-reformer (inlet) temperature. An overview of the simulated stack parameters is provided in Table 5.

The manufacturer advices to control the temperature of the stack by adjusting the cathode air flow. The control objective is a maximum PEN temperature of 850 °C, with a minimum air flow of 40 Nl min^{-1} to ensure proper gas distribution in the stack and avoid oxygen starvation at the cathode. A feedback controller with proportional and integral (PI) gain is implemented in the model to adjust the cathode air flow for each current such that the maximum PEN temperature is achieved [18].

The average stack temperature falls rapidly if the stack current is lower than the minimum required to maintain the maximum PEN temperature for the minimum air flow. As a consequence, the ohmic resistance increases and the electrochemical performance reduces. These conditions are not included in the results, since it is undesirable to operate the stack at these conditions.

3.4.2. System simulations

The system efficiencies are calculated for various fuel utilisations, nominal operating conditions and two scenarios: A constant stack power of 1 kW is assumed in the first scenario, which results in different stack currents and cell voltages for the investigated reforming configurations and global fuel utilisations. The second scenario assumes operation at the minimum stack current required to sustain the stack temperature at the minimum cathode air flow. This results in the maximum cell voltage and, therefore, highest stack efficiencies. An overview of the simulated conditions and scenarios is shown in Table 5.

4. Results and discussion

The results of the three simulation steps are divided in three separate sections: The anode inlet compositions calculated for different system configurations and operating conditions are presented in Section 4.1. The results of the stack simulations are discussed in Section 4.2. First, differences in the stack operating characteristics for the investigated reforming strategies are presented, after which contours plots of the cell voltage and maximum PEN temperature gradients are shown for both nominal and off-design operating conditions. The corresponding system efficiencies at nominal conditions are then presented in Section 4.3.

4.1. Anode inlet composition and temperature

Fig. 5 shows the methane concentrations in the fuel gas for various OC ratios and pre-reformer (inlet) temperatures. The maximum allothermal pre-reformer temperature and adiabatic pre-reformer inlet temperatures are based on an SOFC outlet temperature of 825 °C,

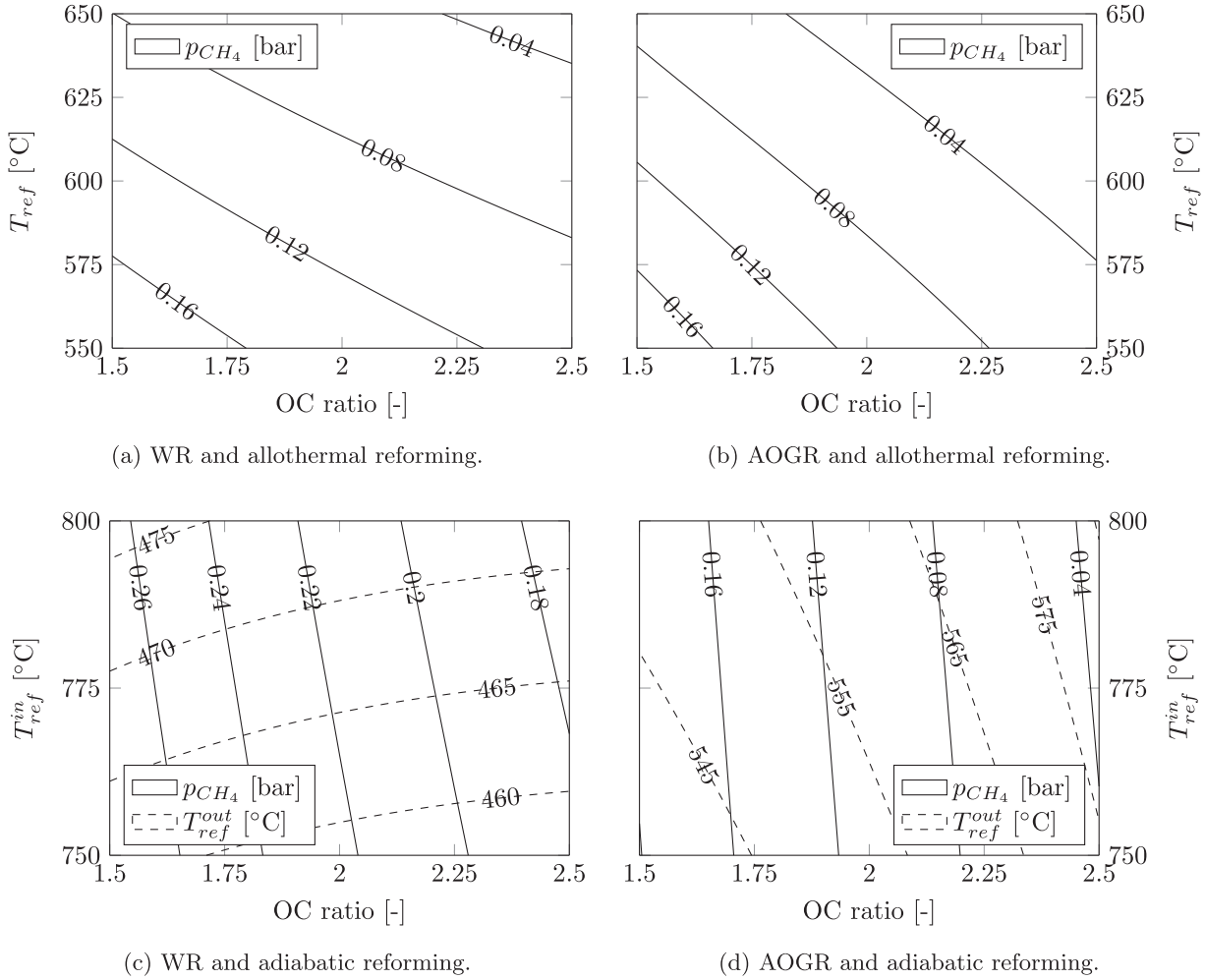

(a) WR and allothermal reforming.

(b) AOGR and allothermal reforming.

(c) WR and adiabatic reforming.

(d) AOGR and adiabatic reforming.

Fig. 5. Contours of methane partial pressures and outlet temperatures of adiabatic pre-reformers for different reforming configurations, OC ratios and reformer (inlet) temperatures.

specified by the stack manufacturer [41,42]. Higher allothermal pre-reformer temperatures may require more heat than available in the exhaust gases, while hardly any methane is reformed at temperatures below 550 °C. Similarly, adiabatic pre-reformer temperatures in excess of 800 °C lead to a low heat transfer rate in the fuel pre-heater.

The selected reforming conditions result in methane partial pressures ranging from less than 0.04, for high OC ratios and reformer temperatures, to over 0.26 for low OC ratios and adiabatic reforming. The differences between the two allothermal reforming cases, shown in Fig. 5a and b respectively, are small. However, AOGR results in slightly lower methane partial pressures compared to WR due to dilution with carbon dioxide. A similar effect can be observed when comparing the two adiabatic pre-reforming cases.

Fig. 5c shows that adiabatic pre-reforming results in substantially higher methane partial pressures than allothermal pre-reforming when WR is used, especially when comparing higher reformer temperatures. For AOGR, shown in Fig. 5d, the methane partial pressures are similar for allothermal and adiabatic pre-reforming. A combination of AOGR and adiabatic pre-reforming results in lower methane partial pressures and higher reformer outlet temperatures than WR and adiabatic pre-reforming.

Fig. 6a shows the *RR* and $u_{f,sp}$ for various OC ratios and global fuel utilisations. The recirculation ratio increases for higher OC ratios and lower global fuel utilisations. This affects the methane partial pressures for AOGR and adiabatic reforming, as can be seen in Fig. 6b. The methane partial pressure decreases for higher recirculation ratios, while the outlet temperature seems more related to the fuel utilisation for a single pass. OC ratios above 2 are commonly used in SOFC systems to suppress carbon deposition.

4.2. Stack simulations

The stack simulations results are presented in three parts: Section 4.2.1 presents the spatial distributions of the reforming rate, current density, temperature and temperature gradient for nominal operating conditions. Contours of the cell voltage and maximum temperature gradients are presented in Section 4.2.2 for various stack currents and fuel utilisations, and Section 4.2.3 presents these contours for various stack currents and other off-design conditions.

4.2.1. Spatial distributions

Fig. 7 shows the simulated distributions of the MSR reaction rate, current density, PEN temperature and PEN temperature gradient from inlet to outlet for the nominal operating condition specified in Table 5. Fig. 7a shows that the MSR rate is initially highest for the WR case with allothermal pre-reforming, while it is more equally distributed when anode off-gas is recirculated. Adiabatic pre-reforming result in lower reformer outlet temperatures, and subsequently reduces the entrance temperature of the stack. Therefore, the MSR is initially lower for the two adiabatic cases.

The current density distribution, shown in Fig. 7b, behaves inversely to the MSR reaction rate: The current density is relatively equally distributed for both the allothermal pre-reforming concepts, but triples from inlet to outlet for the adiabatic pre-reforming. Both the DIR rate and current density distribution have a strong dependency on the local PEN temperature, shown in Fig. 7c.

The PEN temperature drops initially at the inactive inlet section, while heat is transferred from the air to the fuel. The temperature then increases by heat from the electrochemical reaction, mostly conducted via the metallic interconnect. The cold sport at the beginning of the active area is caused by the high local DIR rate. The temperature difference from inlet to outlet is higher for adiabatic than allothermal reforming conditions. In addition, the temperature increases slower for AOGR than WR, due to lower fuel utilisation for a single pass, which increases the fuel flow and reduces concentration losses near the outlet.

Fig. 7d shows the local PEN temperature gradients calculated form the simulated PEN temperature gradients. The difference in the maximum temperature gradient between WR and AOGR is negligible for allothermal pre-reforming, although it occurs somewhat later for AOGR. However, the maximum temperature gradient almost doubles for adiabatic pre-reforming, and is higher for WR than AOGR.

Overall, the simulations show that allothermal pre-reforming results in higher average stack temperatures and smaller temperature gradients than adiabatic pre-reforming, even though the adiabatic pre-reformer inlet temperature assumed is 175 °C higher than the allothermal reforming temperature. However, the stack simulation results are based on an electrochemical model validated for three different fuel composition only. Although the accuracy was shown to be high ($R^2 = 0.99$), the model is not fully validated for various degrees of internal reforming, which should be taken up in future work.

4.2.2. Fuel utilisation

The previous section showed detailed spatial distributions within the stack, but for nominal conditions only. However, fuel utilisations, reformer (inlet) temperature and OC ratios vary in practice. Therefore, a range of off-design conditions is simulated as well. Fig. 8 shows contours for constant simulated cell voltages and maximum PEN temperature gradients for various global fuel utilisations and stack currents for the investigated reforming concepts. Stack currents which are insufficient to maintain the operating temperature of 850 °C at the

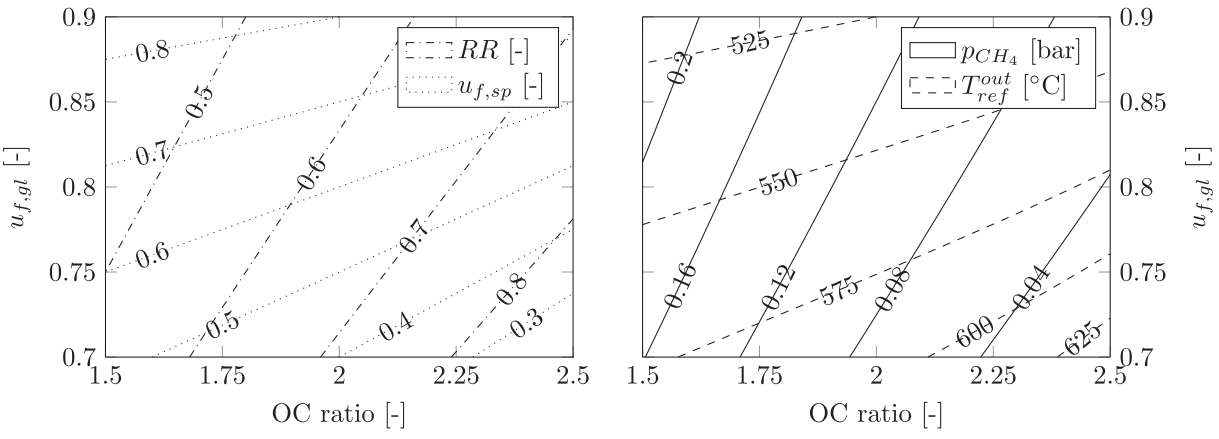

(a) AOGR, all cases. (b) AOGR and adiabatic reforming.

Fig. 6. *RR* and $u_{f,sp}$ (a) and methane partial pressures and adiabatic pre-reformer outlet temperatures (b) for various OC ratios and $u_{f,gl}$ when AOGR is employed, for a reformer inlet temperature of 775 °C.

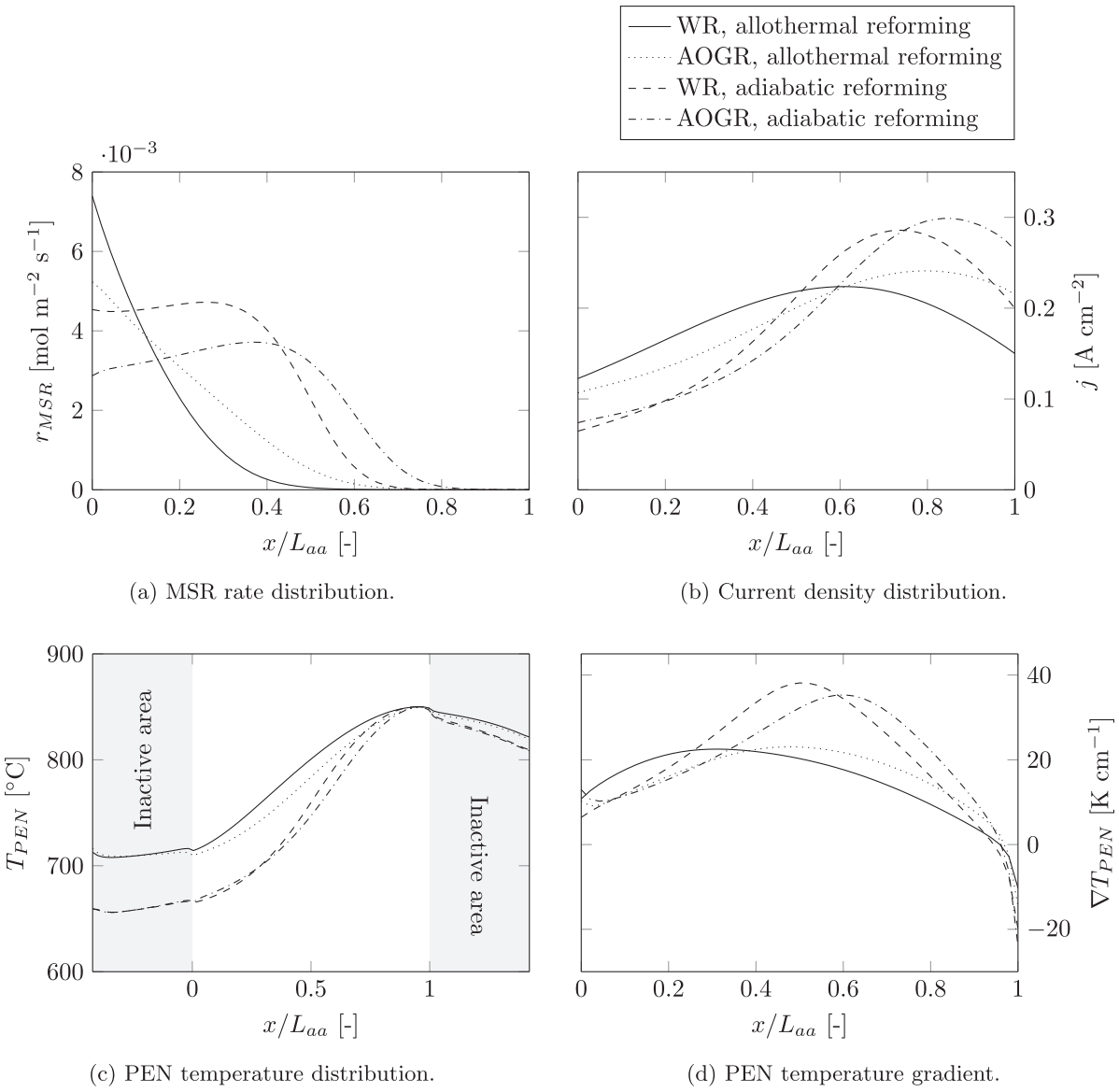

(a) MSR rate distribution.

(b) Current density distribution.

(c) PEN temperature distribution.

(d) PEN temperature gradient.

Fig. 7. Spatial distribution of the MSR rate, current density, PEN temperature and PEN temperature gradient in the SOFC stack for the investigated reforming configurations and the nominal conditions specified in Table 5.

minimum air flow of 40 Nl min^{-1} are not considered.

The cell voltage and maximum PEN temperature gradient are primarily determined by the stack current for the allothermal pre-reforming configuration with WR, and only a weak function of the global fuel utilisation. The effect of the global fuel utilisation is higher in the case of AOGR, since it changes the recirculation ratio: A high recirculation ratio is required to maintain an OC ratio at low fuel utilisations, which cools down the entrance of the stack and increases the temperature gradient from inlet to outlet.

Adiabatic pre-reforming reduces the fuel inlet temperature and increases the methane partial pressure. As a result, lower cell voltages and, subsequently, higher stack currents are required to generate sufficient heat for internal reforming while maintaining the maximum PEN temperature of 850 °C. The increased temperature difference from inlet to outlet results in notably higher temperature gradients in the stack compared to the allothermal pre-reforming case. In addition, the maximum PEN temperature gradient is a strong function of the global fuel utilisation when water is recirculated.

AOGR reduces the cell voltages in the stack in all simulated cases, despite the lower fuel utilisation for a single pass. This is a result of the constant OC assumed in this study, which lowers the hydrogen-to-carbon ratios compared to WR. In practice, the lower single pass fuel utilisation may offer advantages in the fuel distribution within the stack, reducing cell-to-cell variations and allowing higher global fuel utilisations. The 1D model used in this study does, however, not account for cell-to-cell variations.

On the other hand, AOGR reduces the temperature gradients in the stack, especially for adiabatic pre-reforming. This is most effective if the recirculation ratio is low and the single pass fuel utilisation is high, since a high single pass fuel utilisation results in a more homogeneous current density distribution in the stack. The high current density at the hot outlet section of the stack is constrained by the increasing concentration losses for high single pass fuel utilisations.

The cell voltages are generally lower for adiabatic pre-reforming and AOGR than allothermal pre-reforming and WR, which is amplified by the lower cell voltages or higher fuel utilisations required to maintain the desired operating temperature. This reveals the trade of between operating at high current density to increase the power density, lower the specific product costs and reduce thermal stresses, while operating at low current densities increases the stack voltage and the efficiency.

Table 5
Overview of the simulated stack and system operating conditions.

Stack simulations	Unit	Nominal	Range	Interval
Stack current, I_{stack}	[A]	24	15–27	0.5
Fuel utilisation, $u_{f,gl}$	[–]	0.8	0.7–0.9	0.025
Air inlet temperature, T_{air}^{in}	[°C]	725	675–775	10
Allothermal pre-reformer, T_{ref}	[°C]	600	550–650	10
Adiabatic pre-reformer, T_{ref}^{in}	[°C]	775	750–800	5
OC ratio	[–]	2	1.5–2.5	0.1
System simulations				
Global fuel utilisation ($u_{f,gl}$)	varied from 0.7 to 0.9			
T_{air}^{in}, T_{ref}, T_{ref}^{in}, and OC ratio	nominal conditions			
U_{cell} and ∇T_{PEN}^{max}	obtained from stack simulations			
Cases				
(a): Stack power (P_{stack}) of 1 kWe				
(b): Maximum cell voltage (U_{cell}) at minimum cathode air flow (40 Nl min^{-1})				

4.2.3. Other operating conditions

Fig. 9 shows contours of constant cell voltage and maximum PEN temperature gradient for changes in the pre-reformer (inlet) temperature, air inlet temperature and OC ratio. Fig. 9a shows contours for allothermal pre-reformer temperatures from 550 to 650 °C for the system with WR. This result shows that increasing the reformer temperature may reduce the maximum temperature gradient in the stack as much as 5 K cm^{-1}. However, Fig. 9c shows that an increase in the adiabatic pre-reformer inlet temperature has little effect on the maximum temperature gradients in the stack.

Fig. 9b shows that increasing the air temperature increases the cell voltage in the stack and reduces the maximum PEN temperature gradient in a SOFC stack operated with an allothermal pre-reformer and AOGR. Although this may improve SOFC performance, the heat available in the outlet gases should be sufficient to pre-heat the incoming air to the required temperature. In addition, the size and cost of the air pre-heater will consequently increase.

The OC ratio affects stack operation particularly for AOGR, since it determines the recirculation ratio and fuel utilisation for a single pass. Fig. 9d shows that an increase in the OC ratio from 1.5 to 2.5 decreases the cell voltage in the stack, but reduces the temperature gradient in the stack from over 38 to less than 32 K cm^{-1}.

Overall, the results in Fig. 9 demonstrate the capability of the stack model to simulate the off-design performance of a commercial SOFC

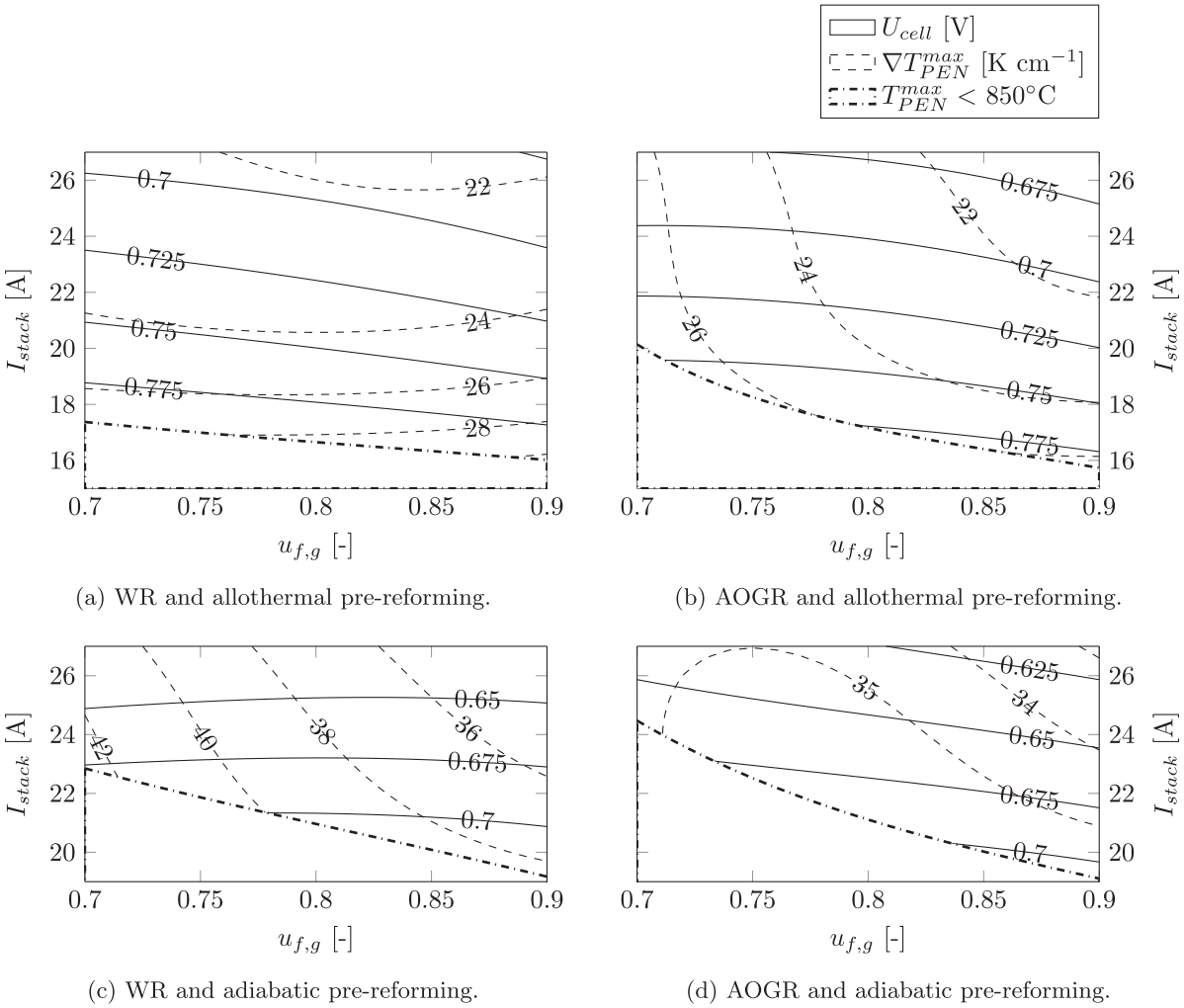

(a) WR and allothermal pre-reforming.

(b) AOGR and allothermal pre-reforming.

(c) WR and adiabatic pre-reforming.

(d) AOGR and adiabatic pre-reforming.

Fig. 8. Cell voltages and maximum PEN temperature gradients in the stack for different reforming configurations, fuel utilisations and stack currents.

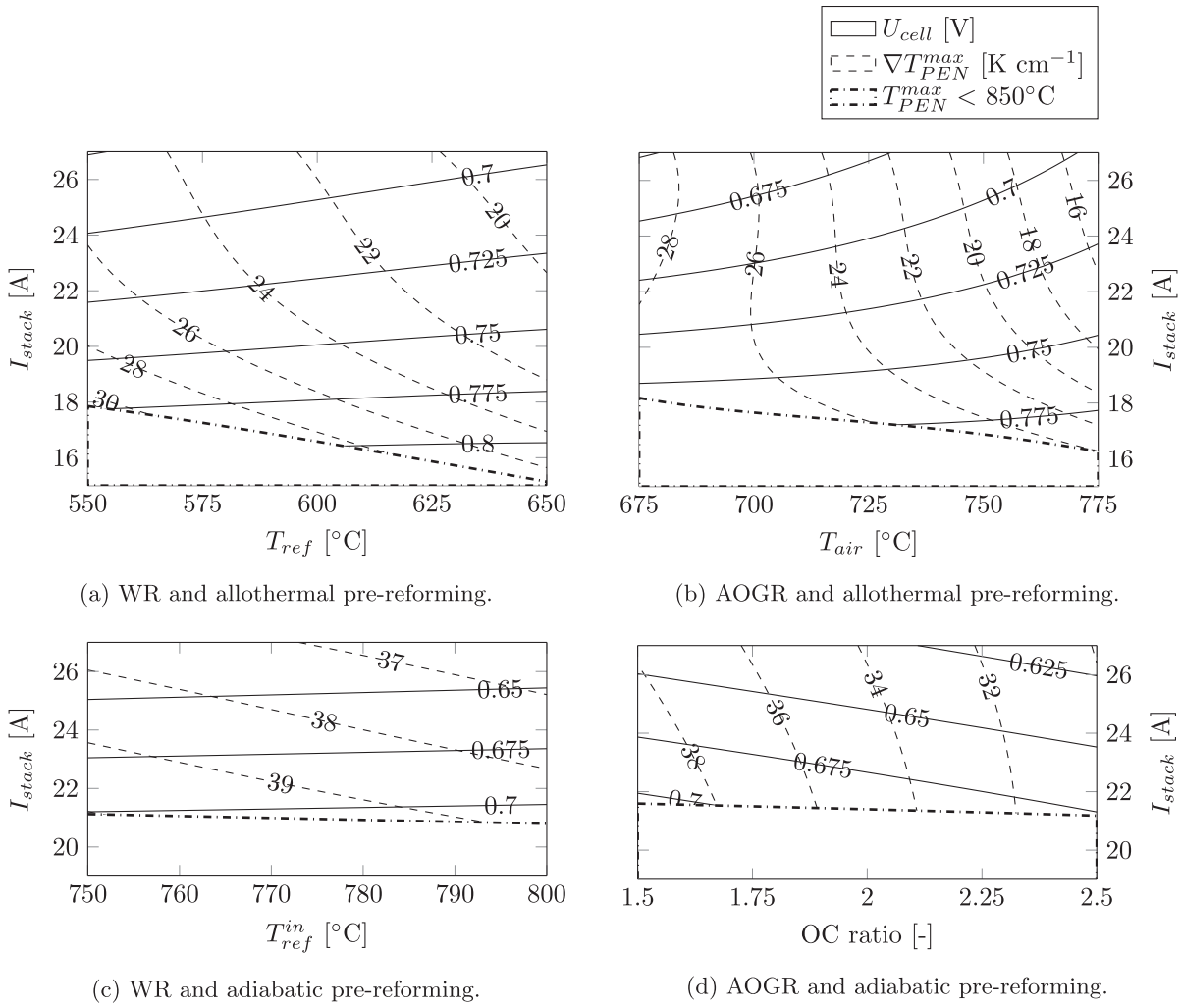

(a) WR and allothermal pre-reforming.

(b) AOGR and allothermal pre-reforming.

(c) WR and adiabatic pre-reforming.

(d) AOGR and adiabatic pre-reforming.

Fig. 9. Cell voltages and maximum PEN temperature gradients in the stack for different reforming configurations and changes in the allothermal pre-reformer temperature (a) and adiabatic pre-reformer inlet temperature (c) for WR and various cathode air inlet temperatures (b) and OC ratios (d) for AOGR.

stack. The changes in the pre-reformer (inlet) temperature, air inlet temperature and OC ratio were simulated for the other investigated reforming concepts as well. These results are included as supplementary material (Figs. S.1 to S.3).

4.3. System simulations

The stack simulations provide detailed insight in the effects of different reforming concepts on the electrochemistry and temperature gradients in the stack. Although the stack efficiency is directly proportional to the cell voltage, the overall system efficiency is affected by the parasitic power consumed by the balance of plant components as well. Therefore, system models are developed to calculate the corresponding system efficiencies.

The system efficiencies are calculated for nominal conditions in two scenarios: A constant stack power of 1 kWe is assumed in the first scenario, to allow a comparison for a similar capital expenditure. The second scenario assumes operation at the lowest current required to support a stack temperature of 850 °C for the minimum air flow of 40 Nl min^{-1}, which results in the maximum cell voltage and stack efficiency.

4.3.1. Constant stack power

Fig. 10 shows the results of the system calculations for a constant stack power of 1 kW and global fuel utilisations from 0.7 to 0.9. Fig. 10a shows that the cell voltages are clearly higher for the cases with allothermal than adiabatic pre-reforming. WR generally yields higher cell voltages than AOGR, except for adiabatic pre-reforming at low fuel utilisations, where the high degree of DIR cools down the stack substantially. As a result, the cell voltage increases with fuel utilisation for WR and adiabatic pre-reforming, while it decreases in all other cases.

The stack efficiency is proportional to the cell voltage and global fuel utilisation, as can be seen in Fig. 10c. For adiabatic reforming at low fuel utilisation, the stack efficiency is consequently lower for WR than AOGR, but higher for fuel utilisations in excess of 0.75. The highest stack efficiency is attained with WR and allothermal pre-reforming, but the difference with WR and adiabatic pre-reforming decreases as the fuel utilisation increases.

The oxygen utilisation is inversely correlated with the cathode air flow, thus a decreasing oxygen utilisation indicates an increase in the parasitic power consumption by the cathode air blower. The oxygen utilisation, shown in Fig. 10b, decreases for lower cell voltages and more pre-reforming, due to the higher air flow required to cool the stack.

Adiabatic pre-reforming reduces the parasitic power consumption by the air blower compared to allothermal reforming. Consequently, the difference between between the net efficiency of systems with adiabatic pre-reforming and allothermal pre-reforming reduces compared to the stack efficiency, as can be seen in Fig. 10d. The net system efficiency with adiabatic pre-reforming and WR even exceeds that of the allothermal pre-reforming and AOGR, despite the higher cell

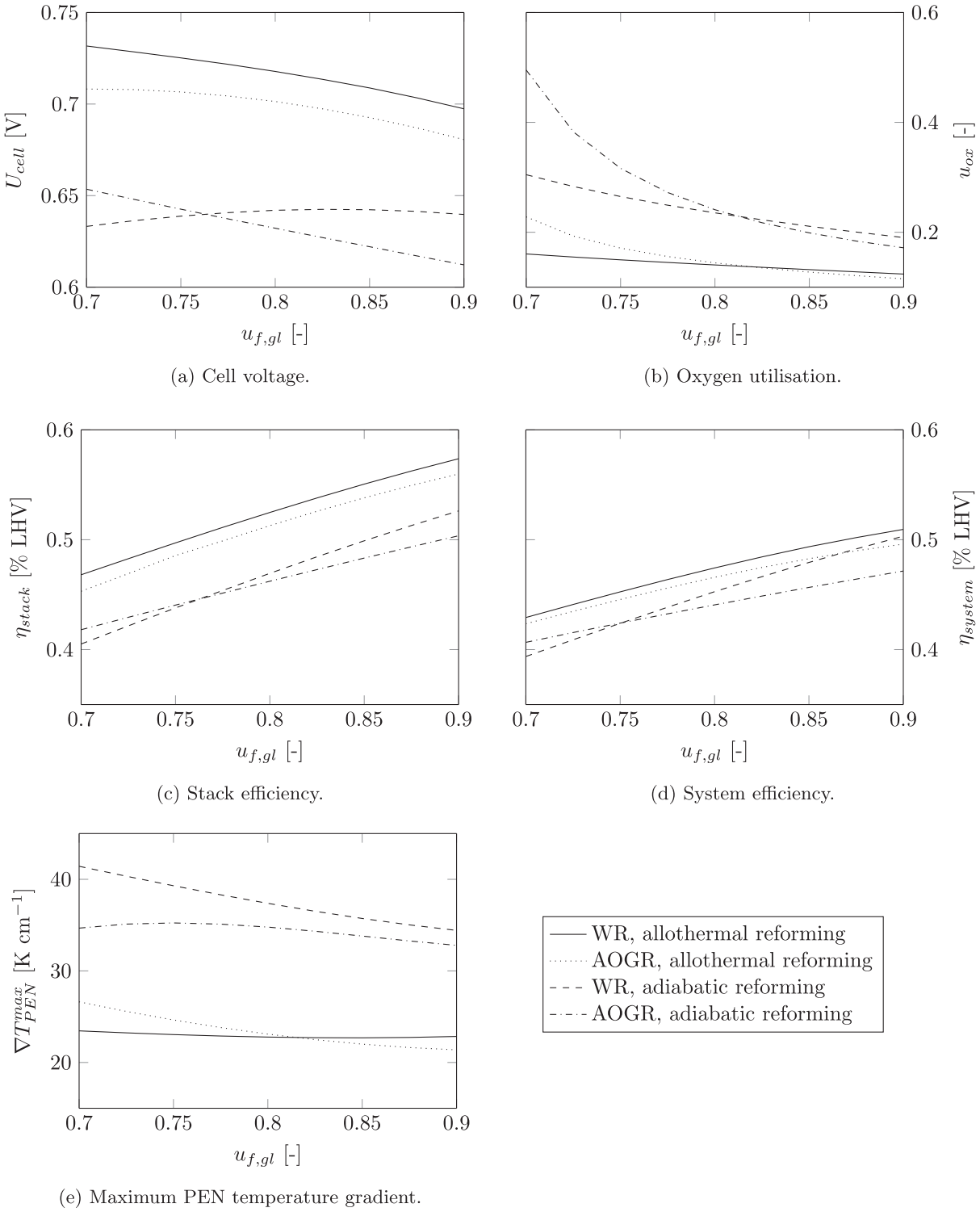

(a) Cell voltage.

(b) Oxygen utilisation.

(c) Stack efficiency.

(d) System efficiency.

(e) Maximum PEN temperature gradient.

Fig. 10. Results of the system simulation for different reforming configurations at reference operating conditions and a constant stack power of 1 kWe.

voltages achieved by the latter.

Higher degrees of internal reforming increase potentially deteriorating temperature gradients in the stack as well. Fig. 10e shows that the PEN temperature gradients are about 10 K cm^{-1} higher for system configurations with adiabatic pre-reforming compared to concepts with allothermal pre-reforming, which may compromise the stack lifetime.

4.3.2. Maximum cell voltage

Fig. 11 presents the results for stack operation at the maximum cell voltage (i.e. minimum cathode air flow) and nominal conditions. Fig. 11a shows that the cell voltage is virtually constant around 0.8 V for the system with allothermal pre-reforming and WR. The cell voltage increases with the fuel utilisation for the other system configurations, as more heat is available to reform the fuel and maintain the stack temperature for the same fuel flow. Similar to the case of constant stack power, the highest cell voltage is obtained with allothermal pre-reforming and WR, and the voltage decreases when adiabatic pre-reforming or AOGR is adopted instead.

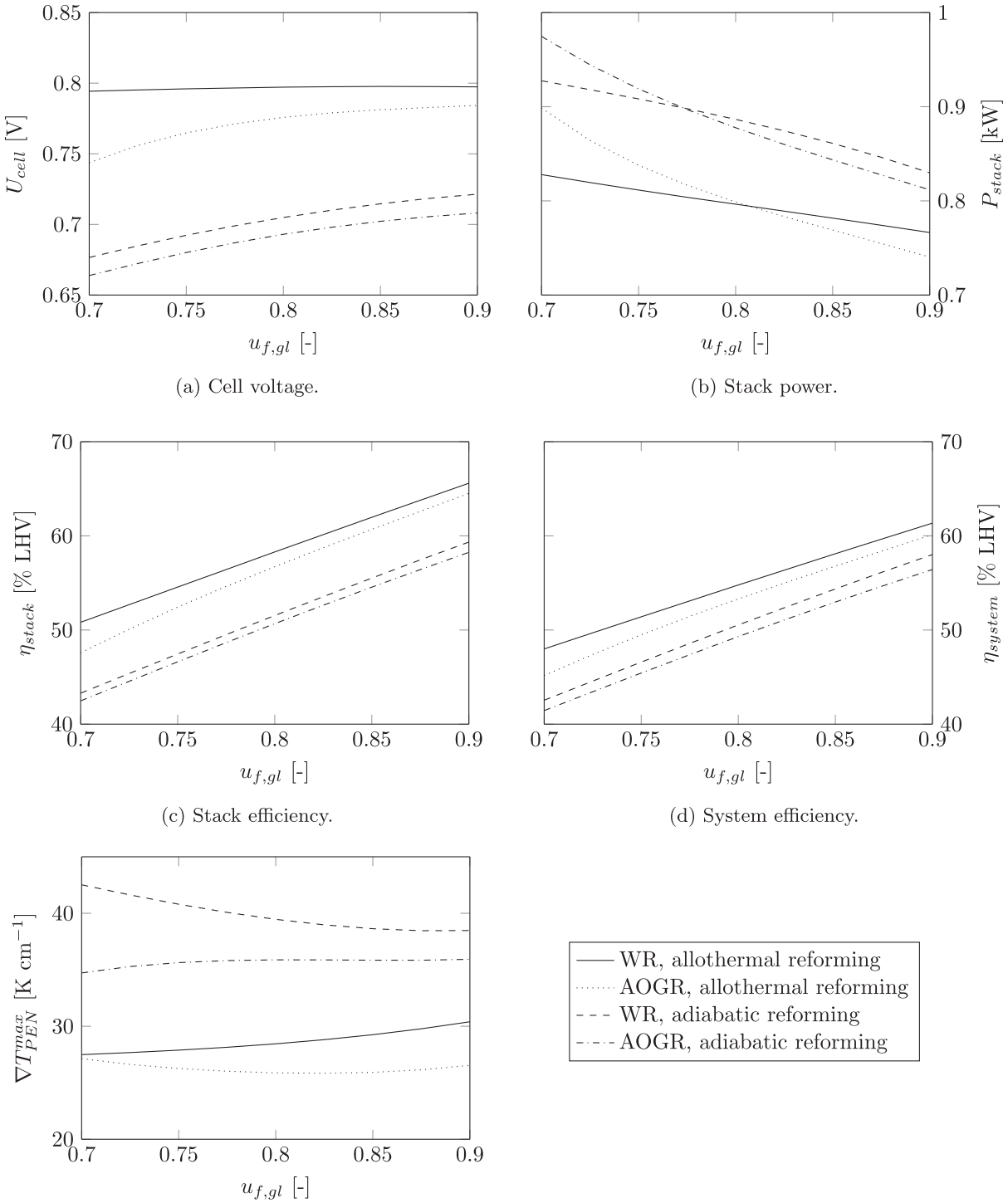

(a) Cell voltage.

(b) Stack power.

(c) Stack efficiency.

(d) System efficiency.

(e) Maximum PEN temperature gradient.

Fig. 11. Results of the system simulation for different reforming configurations at reference operating conditions and the minimum air flow specified by the manufacturer.

Fig. 11c shows that the highest stack efficiency is attained at the maximum fuel utilisation, and decreases proportionally with the cell voltage from 65.6% for allothermal pre-reforming and WR to 58.3% for adiabatic pre-reforming and AOGR, a difference of 7.3% point. The net system efficiency, shown in Fig. 11d, follows a similar trend. However, the maximum system efficiency decreases from 61.4% for allothermal pre-reforming and water recycling to 56.4% for adiabatic pre-reforming and AOGR, a reduction of 5% point only.

High cell voltages enhance both stack and system efficiency, but the low currents reduce the electric power produced by the stack, as can be seen in Fig. 11b. The lower stack currents for allothermal pre-reforming result in substantially lower stack powers compared to adiabatic pre-reforming. Interestingly, AOGR results in higher stack powers for lower fuel utilisations, but this trend reverses for higher fuel utilisations. Therefore, AOGR seems to be most interesting for lower fuel utilisations, since both the power density and stack efficiency reduce

compared to WR for $u_{f,gl} > 0.8$.

Fig. 11e shows that there are substantial differences in the maximum temperature gradients in the stack. Since the air flow is the same for all cases (i.e. the minimum), these differences originate from the magnitude, temperature and composition of the fuel flow or stack current. The maximum temperature gradient increases with fuel utilisation in the WR case for allothermal pre-reforming, but decreases for adiabatic pre-reforming. The lowest temperature gradients are observed for a combination of AOGR and allothermal pre-reforming, while WR and adiabatic pre-reforming result in the highest temperature gradients.

Only heat from the electrochemical reaction is used in the adiabatic pre-reforming cases to reform the fuel, omitting the use of heat produced by an off-gas burner. This limits the heat available for pre-reforming and, therefore, the maximum voltage and minimum fuel utilisation. However, adiabatic reforming is interesting if the fuel or heat can be further utilised, for example in combined heat, hydrogen and power production or hybrid operation with internal combustion engines or low temperature fuel cells.

The ISM assumed this study dissipates 200 to 250 W of heat to the surroundings, depending on the operating conditions. If the fuel is pure hydrogen or fully pre-reformed, this helps to remove the heat produced by the exothermic hydrogen oxidation reaction and avoids excessive cathode air flows. However, the results demonstrate that heat insulation becomes more important if the stack is operated with high degrees of internal reforming, since the minimum air dictates a minimal operating current to sustain the operating temperature, and limits the maximum achievable cell voltage.

Overall, the results demonstrate that an inclusive analysis at both stack and balance of plant level is indispensable to assess the consequences of different reforming concepts in SOFC systems. Stack simulations are required to accurately predict the electrochemical performance of the stack and identify potentially deteriorating operating conditions, but losses in the balance of plant are just as important.

It should be noted that the stack model is only validated for three different fuel compositions. In addition, the calculated system efficiencies are based on literature values. Therefore, further validation of both stack and system models need to be taken up in future work.

5. Conclusions

Four SOFC system configurations, representing different reforming concepts with either allothermal or adiabatic pre-reforming and either WR or AOGR, were analysed on both and stack level. The stack was simulated in detail for the investigated system configurations, to predict the electrochemical performance of the stack as well as temperature gradients in the PEN structures for a range of operating conditions. The results were used to calculate the corresponding system efficiencies.

Adiabatic pre-reforming and AOGR reduce the cell voltage in the stack compared to allothermal pre-reforming and WR at nominal operating conditions. In addition, the temperature gradients increase for adiabatic pre-reforming, due to the lower degree of pre-reforming, and decrease for higher stack currents and global fuel utilisations. The stack needs to be operated at relatively high currents and low cell voltages to maintain the desired operating temperature with high degrees of internal reforming and low fuel utilisations.

The highest system efficiency is obtained for allothermal pre-reforming and WR. However, high stack efficiency not necessarily results in a high system efficiencies. This is, for example, the case when comparing allothermal pre-reforming and AOGR with adiabatic pre-reforming and WR. As expected, a trade-off exists between high system efficiency and stack power. In addition, AOGR improves the power density compared to WR for low fuel utilisations, but yields lower power densities for higher fuel utilisations.

The results demonstrate that both stack and system operation need to be considered to design an efficient SOFC system and predict potentially deteriorating temperature gradients in the stack. However, both stack and system models need to be further validated in future work. Once sufficiently validated, the procedure used in this study may be extended to other stacks, cells, system configurations, operating conditions and fuels.

CRediT authorship contribution statement

L. Biert: Conceptualization, Methodology, Software, Writing - original draft. **K. Visser:** Writing - review & editing, Supervision, Funding acquisition, Project administration. **P.V. Aravind:** Writing - review & editing, Supervision, Funding acquisition, Project administration.

Declaration of Competing Interest

The authors declare that they have no known competing financial interests or personal relationships that could have appeared to influence the work reported in this paper.

Acknowledgements

This research is supported by the project *"GasDrive: Minimizing emissions and energy losses at sea with LNG combined prime movers, underwater exhausts and nano hull materials"* (project 14504) of the Netherlands Organisation for Scientific Research (NWO), domain Applied and Engineering Sciences (TTW).

Appendix A. Supplementary material

Supplementary data associated with this article can be found, in the online version, at https://doi.org/10.1016/j.apenergy.2020.114748.

References

[1] Schellnhuber HJ, Rahmstorf S, Winkelmann R. Why the right climate target was agreed in paris. Nat Clim Change 2016;6(7):649–53.
[2] Gerard D, Lave LB. Implementing technology-forcing policies: The 1970 clean air act amendments and the introduction of advanced automotive emissions controls in the united states. Technol Forecast Soc Chang 2005;72(7):761–78.
[3] Stambouli AB, Traversa E. Fuel cells, an alternative to standard sources of energy. Renew Sustain Energy Rev 2002;6(3):295–304.
[4] Edwards PP, Kuznetsov VL, David WI, Brandon NP. Hydrogen and fuel cells: towards a sustainable energy future. Energy policy 2008;36(12):4356–62.
[5] van Biert L, Godjevac M, Visser K, Aravind P. A review of fuel cell systems for maritime applications. J Power Sources 2016;327:345–64.
[6] Brynolf S, Taljegard M, Grahn M, Hansson J. Electrofuels for the transport sector: a review of production costs. Renew Sustain Energy Rev 2018;81:1887–905.
[7] Peters R, Riensche E, Cremer P. Pre-reforming of natural gas in solid oxide fuel-cell systems. J Power Sources 2000;86(1):432–41.
[8] Liso V, Olesen AC, Nielsen MP, Kær SK. Performance comparison between partial oxidation and methane steam reforming processes for solid oxide fuel cell (SOFC) micro combined heat and power (CHP) system. Energy 2011;36(7):4216–26.
[9] Payne R, Love J, Kah M. Generating electricity at 60% electrical efficiency from 1–2 kWe SOFC products. ECS Trans 2009;25(2):231–9.
[10] van Biert L, Woudstra T, Godjevac M, Visser K, Aravind PV. A thermodynamic comparison of solid oxide fuel cell-combined cycles. J Power Sources 2018;397:382–96. https://doi.org/10.1016/j.jpowsour.2018.07.035.
[11] Laosiripojana N, Assabumrungrat S. Catalytic steam reforming of methane, methanol, and ethanol over Ni/YSZ: the possible use of these fuels in internal reforming SOFC. J Power Sources 2007;163(2):943–51.
[12] Janardhanan VM, Heuveline V, Deutschmann O. Performance analysis of a SOFC under direct internal reforming conditions. J Power Sources 2007;172(1):296–307.
[13] Brett DJL, Atkinson A, Cumming D, Ramírez-Cabrera E, Rudkin R, Brandon NP. Methanol as a direct fuel in intermediate temperature (500–600 °C) solid oxide fuel cells with copper based anodes. Chem Eng Sci 2005;60(21):5649–62.
[14] Laosiripojana N, Assabumrungrat S. Catalytic steam reforming of dimethyl ether (dme) over high surface area ce–zro2 at sofc temperature: The possible use of dme in indirect internal reforming operation (iir-sofc). Appl Catal A: Gen 2007;320:105–13.
[15] Gorte RJ, Kim H, Vohs JM. Novel sofc anodes for the direct electrochemical oxidation of hydrocarbon. J Power Sources 2002;106(1–2):10–5.
[16] Wojcik A, Middleton H, Damopoulos I, et al. Ammonia as a fuel in solid oxide fuel cells. J Power Sources 2003;118(1–2):342–8.
[17] Powell M, Meinhardt K, Sprenkle V, Chick L, McVay G. Demonstration of a highly efficient solid oxide fuel cell power system using adiabatic steam reforming and anode gas recirculation. J Power Sources 2012;205:377–84.

[18] van Biert L, Godjevac M, Visser K, Aravind PV. Dynamic modelling of a direct internal reforming solid oxide fuel cell stack based on single cell experiments. Appl Energy 2019;250:976–90. https://doi.org/10.1016/j.apenergy.2019.05.053.
[19] Peters R, Deja R, Blum L, Pennanen J, Kiviaho J, Hakala T. Analysis of solid oxide fuel cell system concepts with anode recycling. Int J Hydrogen Energy 2013;38(16):6809–20.
[20] Ahmed K, Föger K. Perspectives in solid oxide fuel cell-based microcombined heat and power systems. J Electrochem Energy Convers Storage 2017;14(3):031005.
[21] Engelbracht M, Peters R, Blum L, Stolten D. Comparison of a fuel-driven and steam-driven ejector in solid oxide fuel cell systems with anode off-gas recirculation: Part-load behavior. J Power Sources 2015;277:251–60.
[22] Dolenc B, Vrecko D, Juricic D, Pohjoranta A, Kiviaho J, Pianese C. Soft sensor design for estimation of sofc stack temperatures and oxygen-to-carbon ratio. ECS Trans 2015;68(1):2625–36.
[23] Halinen M. Improving the performance of solid oxide fuel cell systems; 2015.
[24] Chen J, Liang M, Zhang H, Weng S. Study on control strategy for a sofc-gt hybrid system with anode and cathode recirculation loops. Int J Hydrogen Energy 2017;42(49):29422–32.
[25] Engelbracht M, Peters R, Blum L, Stolten D. Analysis of a solid oxide fuel cell system with low temperature anode off-gas recirculation. J Electrochem Soc 2015;162(9):F982–7.
[26] Riensche E, Meusinger J, Stimming U, Unverzagt G. Optimization of a 200 kW SOFC cogeneration power plant. part II: variation of the flowsheet. J Power Sources 1998;71(1):306–14.
[27] Genc O, Toros S, Timurkutluk B. Determination of optimum ejector operating pressures for anodic recirculation in sofc systems. Int J Hydrogen Energy 2017;42(31):20249–59.
[28] Genc O, Toros S, Timurkutluk B. Geometric optimization of an ejector for a 4 kw sofc system with anode off-gas recycle. Int J Hydrogen Energy 2018;43(19):9413–22.
[29] Polverino P, Sorrentino M, Pianese C. A model-based diagnostic technique to enhance faults isolability in solid oxide fuel cell systems. Appl Energy 2017;204:1198–214.
[30] Kupecki J, Milewski J, Szczesniak A, Bernat R, Motylinski K. Dynamic numerical analysis of cross-, co-, and counter-current flow configuration of a 1 kw-class solid oxide fuel cell stack. Int J Hydrogen Energy 2015;40(45):15834–44.
[31] Kupecki J, Motylinski K, Milewski J. Dynamic analysis of direct internal reforming in a sofc stack with electrolyte-supported cells using a quasi-1d model. Appl Energy 2017.
[32] Kupecki J, Motylinski K, Milewski J. Dynamic modelling of the direct internal reforming (dir) of methane in 60-cell stack with electrolyte supported cells. Energy Procedia 2017;105:1700–5.
[33] Greco A, Sorce A, Littwin R, Costamagna P, Magistri L. Reformer faults in sofc systems: Experimental and modeling analysis, and simulated fault maps. Int J Hydrogen Energy 2014;39(36):21700–13.
[34] Sorce A, Greco A, Magistri L, Costamagna P. Fdi oriented modeling of an experimental sofc system, model validation and simulation of faulty states. Appl Energy 2014;136:894–908.
[35] Nehter P, Wildrath B, Bauschulte A, Leites K. Diesel based sofc demonstrator for maritime applications. ECS Trans 2017;78(1):171–80.
[36] Rechberger J, Schauperl R, Hansen JB, Larsen PK. Development of a methanol sofc apu demonstration system. ECS Trans 2009;25(2):1085–92.
[37] van Biert L, Visser K, Aravind P. Intrinsic methane steam reforming kinetics on nickel-ceria solid oxide fuel cell anodes. J Power Sources 2019;443:227261.
[38] Woudstra N, Van der Stelt T, Hemmes K. The thermodynamic evaluation and optimization of fuel cell systems. J Fuel Cell Sci Technol 2006;3(2):155–64.
[39] De Groot A. Advanced exergy analysis of high temperature fuel cell systems [PhD thesis]. TU Delft, Delft University of Technology; 2004.
[40] Offer GJ, Mermelstein J, Brightman E, Brandon NP. Thermodynamics and kinetics of the interaction of carbon and sulfur with solid oxide fuel cell anodes. J Am Ceram Soc 2009;92(4):763–80.
[41] Staxera GmbH (D). Technical Documentation Integrated Stack Module (ISM). Technical report available at the web site http://www.fuelcellmarkets.com/content/images/articles/00864_AS_Dokumentation_ISM.pdf [accessed: 2018-10-09].
[42] Staxera GmbH (D). SOFC stack modules for decentralized power generation. Presentation available at the web site https://www.h2fc-fair.com/hm10/images/pdf/staxera01.pdf [accessed: 2018-10-09].
[43] Aguiar P, Adjiman C, Brandon NP. Anode-supported intermediate temperature direct internal reforming solid oxide fuel cell. i: model-based steady-state performance. J Power Sources 2004;138(1):120–36.
[44] Costamagna P, Selimovic A, Del Borghi M, Agnew G. Electrochemical model of the integrated planar solid oxide fuel cell (IP-SOFC). Chem Eng J 2004;102(1):61–9.